VIP Batteries Very Important Paper

International Edition: DOI: 10.1002/anie.201709351
German Edition: DOI: 10.1002/ange.201709351

Singlet Oxygen during Cycling of the Aprotic Sodium–O_2 Battery

*Lukas Schafzahl[+], Nika Mahne[+], Bettina Schafzahl, Martin Wilkening, Christian Slugovc, Sergey M. Borisov, and Stefan A. Freunberger**

Abstract: *Aprotic sodium–O_2 batteries require the reversible formation/dissolution of sodium superoxide (NaO_2) on cycling. Poor cycle life has been associated with parasitic chemistry caused by the reactivity of electrolyte and electrode with NaO_2, a strong nucleophile and base. Its reactivity can, however, not consistently explain the side reactions and irreversibility. Herein we show that singlet oxygen ($^1O_2$) forms at all stages of cycling and that it is a main driver for parasitic chemistry. It was detected in- and ex-situ via a $^1O_2$ trap that selectively and rapidly forms a stable adduct with $^1O_2$. The $^1O_2$ formation mechanism involves proton-mediated superoxide disproportionation on discharge, rest, and charge below ca. 3.3 V, and direct electrochemical $^1O_2$ evolution above ca. 3.3 V. Trace water, which is needed for high capacities also drives parasitic chemistry. Controlling the highly reactive singlet oxygen is thus crucial for achieving highly reversible cell operation.*

The need to advance batteries beyond the limits of current technology in terms of energy, sustainability, and cost has generated immense interest in rechargeable aprotic metal–O_2 batteries.[1] They store charge at the cathode by reversibly forming/decomposing Li_2O_2 or NaO_2 in the Li–O_2 or Na–O_2 cell, respectively. Despite the lower theoretical specific capacity of 488 mAh g^{-1} of NaO_2 and lower voltage of 2.27 V (vs. 1168 mAh g^{-1} at 2.96 V for Li–O_2), the Na–O_2 cell has been reported to have significant advantages over Li–O_2 with respect to rechargeability and energy efficiency.[2] Realizing the Na–O_2 cell, however, still faces many challenges in practice, including the Na-metal anode, lower than theoretical cathode capacity, and perhaps most importantly, insufficient cycle life associated with parasitic chemistry (that is, side reactions) at the cathode.[2,3]

Since the very first papers published on Na–O_2 batteries, superoxide has been perceived responsible for parasitic chemistry with electrolyte and electrode.[1c,3,4] A key measure for parasitic chemistry is the ratio of e^- passed to O_2 consumed/evolved. During discharge, this ratio is typically at the ideal value of one despite approximately 5% of the expected NaO_2 being missing and replaced by side products, such as Na_2CO_3, Na acetate, and Na formate. During subsequent resting and charge, more of these side products form and typically the e^-/O_2 ratio deviates by several percent from one.[2a,3c,4b,5] Although less side products form than in the Li–O_2 cell, cyclability is similarly poor: restricted capacity can often be maintained for up to hundreds of cycles albeit at the expense of true energy, but at full discharge cells fail within some 10 cycles and capacity fading becomes significantly worse with rising charge cut-off voltage.[1c,2a,c,d,3a,d,6]

Superoxide's potential reactivity towards organic substrates stems from its nucleophilicity, basicity, and radical nature, which may cause nucleophilic substitutions, H^+ and H-atom abstraction.[7] Theoretical work, however, has revealed that all these reactions are unlikely with commonly used ether electrolytes owing to the high activation energies and strong endothermicity.[8] Also, the extent of parasitic chemistry at the various stages of cycling does not match the abundance of superoxide. Overall, the reactivity of superoxide cannot consistently explain the observed parasitic chemistry, which thus may only be inhibited with better knowledge about reactive species and their formation mechanism.

Herein we show that singlet oxygen ($^1\Delta_g$ or $^1O_2$), the first excited state of ground state triplet oxygen ($^3\Sigma_g^-$ or $^3O_2$), is the reactive species, which drives parasitic reactions. It is generated at all stages of cycling in relative quantities resembling the occurrence of side reactions: relatively little during discharge, rest, and low charging voltages, and strongly increasing amounts at higher charging voltages.

Methods to sensitively detect $^1O_2$ rely on chemical probes, which selectively react with $^1O_2$. Probes include spin traps and fluorophores, which become EPR active or fluorescing upon reaction with $^1O_2$.[9] However, these probes are not electrochemically inert in the relevant potential range between approximately 2 and 3.6 V versus Na/Na$^+$ and may react with superoxide. Previously, we have shown that 9,10-dimethylanthracene (DMA) fulfills all the requirements;[10] it is stable in contact with superoxide, reacts rapidly with $^1O_2$ to its endoperoxide (DMA-O_2), and has a sufficiently wide potential window (Figure S1 and Scheme S1 in the Supporting Information). $^1O_2$ can either be monitored by DMA consumption via its absorbance or fluorescence between 300 and

[*] L. Schafzahl,[+] N. Mahne,[+] B. Schafzahl, Prof. M. Wilkening, Prof. C. Slugovc, Dr. S. A. Freunberger
Institute for Chemistry and Technology of Materials
Graz University of Technology
Stremayrgasse 9, 8010 Graz (Austria)
E-mail: freunberger@tugraz.at

Prof. S. M. Borisov
Institute for Analytical Chemistry and Food Chemistry
Graz University of Technology
Stremayrgasse 9, 8010 Graz (Austria)

[+] These authors contributed equally to this work.

Supporting information and the ORCID identification number(s) for the author(s) of this article can be found under: https://doi.org/10.1002/anie.201709351.

500 nm (Figure S2), or by detecting DMA and DMA-O_2 via HPLC.

To probe whether $^1O_2$ would form during discharge and charge we constructed Na–O_2 cells as detailed in the Methods Section of the Supporting Information with 0.5 M $NaSO_3CF_3$ (NaOTf) in diglyme containing 40 ppm H_2O and 30 mM DMA as the electrolyte. Water was used because it is required as a phase-transfer catalyst to allow large NaO_2 particles to grow.[2c] To specifically probe reactions at the cathode and to exclude unwanted reactions of electrolyte components with a Na-metal anode, we used the Na intercalation material $Na_{3-x}V_2(PO_4)_3$ as the counter electrode. It operates at approximately 3.4 V versus Na/Na^+ and is thus well within the stability window of the electrolyte.[11] Cells were run at constant current to various states of discharge or charge, then stopped, and the electrolyte extracted and analyzed using HPLC (Figure 1).

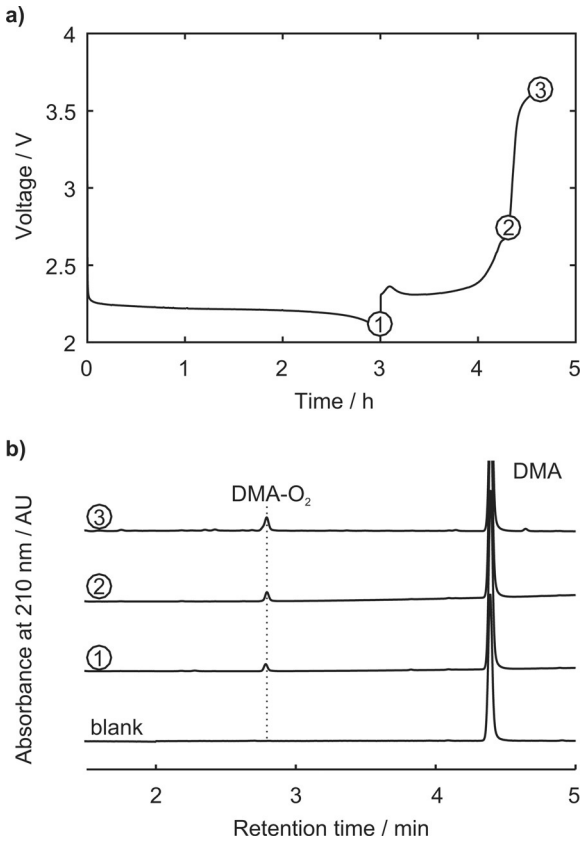

Figure 1. a) Load curve for galvanostatic cycling of a carbon-paper cathode at 90 μA cm^{-2} in 0.5 M NaOTf in diglyme containing 40 ppm H_2O and 30 mM DMA. b) HPLC runs of electrolyte samples taken at the points ①, ②, and ③ in (a), showing $^1O_2$ to have formed as indicated by the conversion of DMA into DMA-O_2. The blank sample was extracted from a cell that rested for 5 h.

The cycle curve shows flat discharge and charge plateaus at approximately 2.2 and 2.3 V, respectively, with a sharp rise in voltage when recharge approaches about 55 % (Figure 1 a). X-ray diffraction confirms that the cube-shaped discharge product is NaO_2 (Figure S3, S4) in accord with many previous reports on similar cells.[1b,c,2a,b,3a] After discharge or recharge to 2.8 and 3.65 V, 4.1, 4.3, and 7.2 %, respectively, of the DMA at the sample points ①, ②, and ③ was converted into DMA-O_2 (Figure 1 b). The amounts of DMA-O_2 equate to 1.4, 1.3, and 2.1 % of the O_2 involved based on the charge at these stages of cycling to have turned into $^1O_2$. $^1O_2$ is thus generated both on discharge and charge, and charging to higher voltage yields significantly more $^1O_2$.

Operando spectroscopy is well suited to probe in detail onset potentials and reaction rates. An operando fluorescence set-up as detailed in the Supporting Information was constructed. Briefly, it consisted of a gas-tight quartz cuvette with a carbon paper working electrode and $Na_{3-x}V_2(PO_4)_3$ as counter and reference electrode and an O_2 filled head space. The O_2-saturated electrolyte was the same as before except for a lower DMA concentration (1.6×10^{-5} M), which best suits fluorescence detection (see the Supporting Information). Excitation and emission wavelengths were chosen according to the maxima in the respective spectra (Figure S2).

While cells as in Figure 1 comprising a porous separator sandwiched between working and counter electrode typically yield NaO_2, cycling the cathode in the operando setup yielded $Na_2O_2{\cdot}H_2O$ as can be inferred from the high charging voltage (Figure S5). Rather similar thermodynamics of NaO_2 and Na_2O_2 ($E^0_{O_2/NaO_2}=2.27$ V, $E^0_{O_2/Na_2O_2}=2.33$ V) were used to explain that the Na–O_2 cell could yield both as a discharge product.[1b,3b] Proton sources decisively influence the discharge product, yet the precise governing factors are unknown.[1b] The reason for peroxide rather than superoxide as a discharge product in the operando setup may be the large electrolyte-to-electrode volume ratio and the stirred electrolyte, both of which are essential for the method. The electrolyte after discharge in the operando setup also contains DMA-O_2, revealing that discharge to Na_2O_2 also forms $^1O_2$ (Figure S6).

To investigate charging of NaO_2, we first discharged a cathode in the standard cell and then placed it in the operando cell. Figure 2 shows the DMA concentration and consumption rate for stepwise potentiostatic charging up to 3.7 V. As soon as the cell was polarized to charging potentials, DMA was consumed at an initially moderate rate, which sharply increased beyond a voltage of about 3.3 V. Thermodynamically, $^1O_2$ can be expected to form upon electrochemically oxidizing NaO_2 above $E^0_{O_2/NaO_2}+E(^1\Delta_g\leftarrow{}^3\Sigma^-_g)$. With 0.97 eV energy difference between $^1O_2$ and $^3O_2$ the thermodynamic threshold to evolve $^1O_2$ can be estimated to be 3.24 V. $^1O_2$ forming at high rate above approximately 3.3 V can thus be explained by the reaction $NaO_2\rightarrow Na^+ + e^- + {}^1O_2$ beyond the thermodynamic threshold of 3.24 V. Up to 3.3 V the $^1O_2$ fraction is around 0.75 to 1.1 % of the expected O_2 (Figure S7). Beyond 3.3 V this fraction increases steadily to around 4 %.

Previously it was reported that most parasitic chemistry occurs during discharge and less on charge.[2a,3a] Charging above around 3.5 V caused the number of O_2 per e^- evolved to deviate more significantly from one than at lower voltages. Correlating these findings with the results in Figure 1, Figure 2, and Figure S7 suggests that parasitic chemistry in the Na–O_2 cathode is closely related to $^1O_2$ formation since

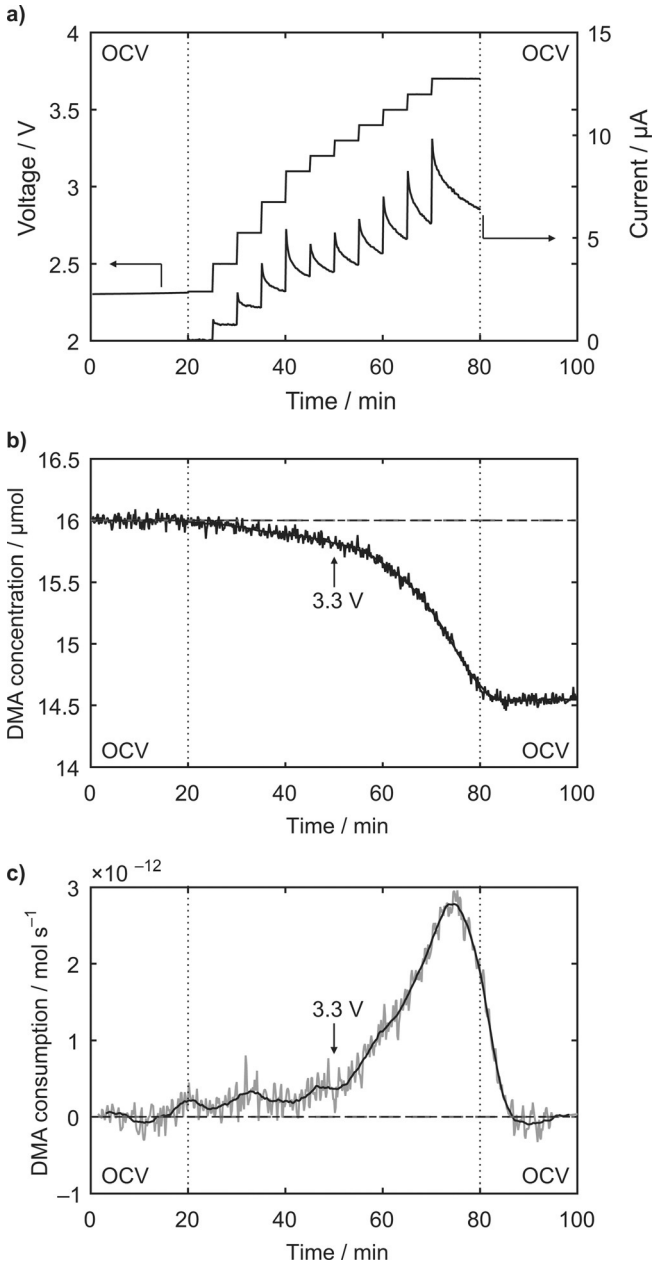

Figure 2. Operando fluorescence detection of $^1O_2$ during potentiostatic charging of a Na–O_2 cathode. The carbon-paper cathode was first discharged in a Swagelok type cell to 75 mAh cm^{-2} in 0.5 M NaOTf in diglyme containing 40 ppm H_2O and then introduced into the operando setup containing the same electrolyte and additionally 1.6×10^{-5} M DMA. a) Voltage and current profile. b) DMA concentration. c) DMA consumption rate.

the extent of side reactions follows the occurrence of $^1O_2$: $^1O_2$ is formed at a higher rate during discharge than at charging below 3.3 V and at much higher rate above 3.3 V. In quantitative terms the 1.4% $^1O_2$ during discharge and an approximately 95% yield of NaO_2 suggests a significant fraction of the side products stem from $^1O_2$. Measured $^1O_2$ amounts represents a lower bound since at the low DMA concentration not necessarily all $^1O_2$ will react with DMA and may undergo other decay routes, such as reactions with cell components.

While thermodynamics directly explains how $^1O_2$ forms when NaO_2 is oxidized above 3.3 V, its formation during discharge and recharge below 3.3 V is more surprising. With the Li–O_2 cell, disproportionation of the LiO_2 intermediate to Li_2O_2 was suggested as a major $^1O_2$ source during discharge and low charging voltages.[10] This pathway is inactive in the Na–O_2 cell since discharge stops at NaO_2. When, however, water or other proton sources are present, oxygen reduction will lead to HOO$^\bullet$.[12] This soluble species enables proton-assisted phase-transfer catalysis, which allows the typical micron-sized NaO_2 cubes to grow on discharge and to be oxidized on charge; HOO$^\bullet$ is soluble and mobile in the electrolyte and precipitates NaO_2 via the metathesis reaction $HOO^\bullet + Na^+ \rightleftarrows NaO_2 + H^+$.[2c,13] HOO$^\bullet$, however, can be reduced by superoxide or disproportionate according to Equation (1) and (2),[12] which both have been shown to release $^1O_2$.[14]

$$HOO^\bullet + O_2^- \rightarrow HO_4^- \rightarrow HOO^- + {}^1O_2 \quad (1)$$

$$2\,HOO^\bullet + H_2O \rightarrow H_2O_4 + H_2O \rightarrow H_2O_2 + H_2O + {}^1O_2 \quad (2)$$

That water is driving these reactions is supported by significantly less $^1O_2$ being formed with dry electrolyte as compared to wet electrolyte (Figure S8).

These reactions may not only take place during discharge, where new superoxide is generated, but also at rest since the metathesis reaction is an equilibrium and allows NaO_2 to redissolve into HOO$^\bullet$. A number of studies have shown instability of NaO_2 upon prolonged rest.[3c,4,5] Although details vary, they generally report gradual conversion of NaO_2 into $Na_2O_2{\cdot}H_2O$ accompanied by electrolyte degradation to form NaOH, Na_2CO_3, and organic compounds including Na formate and acetate. Explanations included nucleophilic attack, H^+ and H-atom abstraction by superoxide. To probe how $^1O_2$ is involved in forming the parasitic products we first discharged electrodes in DMA-free electrolyte and then placed them for various times in electrolyte containing 30 mM DMA. X-ray diffraction after storage shows decreased NaO_2 and side products to have formed in accord with previous studies (Figure S9). The electrolyte was then analyzed for DMA-O_2 and the electrodes were analyzed for Na_2CO_3 content by immersing them in 0.1M H_2SO_4 and monitoring the CO_2 evolved by mass spectrometry (Figure 3). $^1O_2$ as indicated by the presence of DMA-O_2 continuously increases with resting time as does the Na_2CO_3 content, which serves as an indication for the extent of parasitic products.

DMA-O_2 and Na_2CO_3 roughly increase proportional to the square root of the resting time, which means that the formation rate decreases with time. The formed parasitic products thus partly passivate the NaO_2 surface and slow down further decomposition. A larger amount of DMA-O_2 than additional Na_2CO_3 formed, which can be explained by two phenomena. First, $^1O_2$ trapped by DMA does not react with cell components and would thus have led to even more parasitic products without DMA. Second, other compounds than Na_2CO_3 will form which are not expelled by acid. Overall, Figure 3 shows that the previously reported electro-

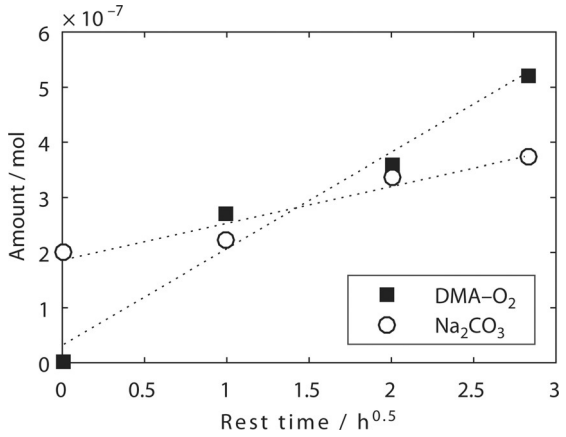

Figure 3. $^1O_2$ generation and parasitic chemistry during prolonged contact of the discharge product NaO_2 with the electrolyte. Cells were first discharged in DMA-free electrolyte (0.5 M NaOTf in diglyme containing 40 ppm H_2O), then the cathodes washed and immersed in the same electrolyte containing additionally 30 mM DMA. After the times indicated the electrolyte was analyzed for DMA-O_2 and the electrodes for Na_2CO_3. The dotted lines are linear fits versus the square root of rest time.

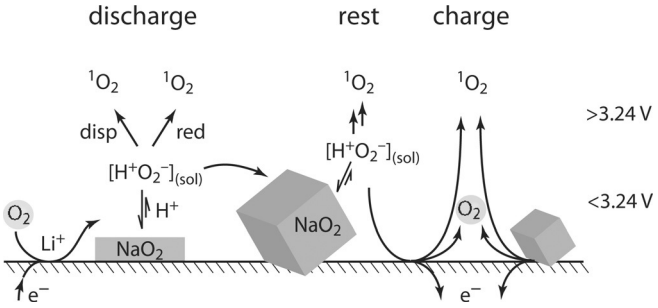

Scheme 1. Pathways leading to $^1O_2$ during discharge, rest, and charge. "Disp" = disproportionation and "red" = reduction.

lyte degradation upon resting is significantly driven by $^1O_2$ formation.

Pathways to $^1O_2$ during discharge, rest, and charge are summarized in Scheme 1. We suggest proton mediated superoxide disproportionation or reduction to interfere with the metathesis equilibrium $HOO^{\bullet} + Na^+ \rightleftarrows NaO_2 + H^+$ as a universal path to $^1O_2$ during all stages of cycling. Upon charge at voltages exceeding the thermodynamic threshold of 3.24 V $^1O_2$ evolves by direct electrochemical oxidation according to $NaO_2 \rightarrow Na^+ + e^- + {}^1O_2$.

In conclusion we demonstrate that singlet oxygen forms at the cathode of the Na–O_2 cell during all stages of cycling and during rest, and accounts for a significant fraction of the side-products formed. $^1O_2$ is thus a major hurdle in cycling the Na–O_2 cell via the reversible formation/decomposition of NaO_2. Water takes up an ambivalent role by being required for high capacity via solution-mediated growth and dissolution of large NaO_2 deposits, and at the same time appearing to be the main driver for $^1O_2$ formation during discharge and at low charging voltages. Future work should thus focus on finding ways to either prevent $^1O_2$ formation or to efficiently eliminate it.

Acknowledgements

S.A.F. is indebted to the European Research Council (ERC) under the European Union's Horizon 2020 research and innovation programme (grant agreement No 636069) and the Austrian Federal Ministry of Science, Research and Economy and the Austrian Research Promotion Agency (grant No. 845364). We thank G. Strohmeier for help with the HPLC measurement, and J. Schlegl for manufacturing instrumentation for the methods used.

Conflict of interest

The authors declare no conflict of interest.

Keywords: electrochemistry · Na–O_2 batteries · parasitic reactions · reaction mechanisms · singlet oxygen

How to cite: *Angew. Chem. Int. Ed.* **2017**, *56*, 15728–15732
Angew. Chem. **2017**, *129*, 15934–15938

[1] a) D. Aurbach, B. D. McCloskey, L. F. Nazar, P. G. Bruce, *Nat. Energy* **2016**, *1*, 16128; b) C. L. Bender, D. Schröder, R. Pinedo, P. Adelhelm, J. Janek, *Angew. Chem. Int. Ed.* **2016**, *55*, 4640–4649; *Angew. Chem.* **2016**, *128*, 4716–4726; c) P. Hartmann, C. L. Bender, M. Vračar, A. K. Dürr, A. Garsuch, J. Janek, P. Adelhelm, *Nat. Mater.* **2012**, *12*, 228–232.

[2] a) B. D. McCloskey, J. M. Garcia, A. C. Luntz, *J. Phys. Chem. Lett.* **2014**, *5*, 1230–1235; b) R. Morasch, D. G. Kwabi, M. Tulodziecki, M. Risch, S. Zhang, Y. Shao-Horn, *ACS Appl. Mater. Interfaces* **2017**, *9*, 4374–4381; c) C. Xia, R. Black, R. Fernandes, B. Adams, L. F. Nazar, *Nat. Chem.* **2015**, *7*, 496–501; d) I. Landa-Medrano, C. Li, N. Ortiz-Vitoriano, I. Ruiz de Larramendi, J. Carrasco, T. Rojo, *J. Phys. Chem. Lett.* **2016**, *7*, 1161–1166.

[3] a) P. Hartmann, C. L. Bender, J. Sann, A. K. Durr, M. Jansen, J. Janek, P. Adelhelm, *Phys. Chem. Chem. Phys.* **2013**, *15*, 11661–11672; b) C. L. Bender, P. Hartmann, M. Vračar, P. Adelhelm, J. Janek, *Adv. Energy Mater.* **2014**, *4*, 1301863; c) S. Y. Sayed, K. P. C. Yao, D. G. Kwabi, T. P. Batcho, C. V. Amanchukwu, S. Feng, C. V. Thompson, Y. Shao-Horn, *Chem. Commun.* **2016**, *52*, 9691–9694; d) M. He, K. C. Lau, X. Ren, N. Xiao, W. D. McCulloch, L. A. Curtiss, Y. Wu, *Angew. Chem. Int. Ed.* **2016**, *55*, 15310–15314; *Angew. Chem.* **2016**, *128*, 15536–15540.

[4] a) J. Kim, H. Park, B. Lee, W. M. Seong, H.-D. Lim, Y. Bae, H. Kim, W. K. Kim, K. H. Ryu, K. Kang, *Nat. Commun.* **2016**, *7*, 10670; b) T. Liu, G. Kim, M. T. L. Casford, C. P. Grey, *J. Phys. Chem. Lett.* **2016**, *7*, 4841–4846.

[5] I. Landa-Medrano, R. Pinedo, X. Bi, I. Ruiz de Larramendi, L. Lezama, J. Janek, K. Amine, J. Lu, T. Rojo, *ACS Appl. Mater. Interfaces* **2016**, *8*, 20120–20127.

[6] S. A. Freunberger, *Nat. Energy* **2017**, *2*, 17091.

[7] a) D. T. Sawyer, J. S. Valentine, *Acc. Chem. Res.* **1981**, *14*, 393–400; b) D. Aurbach, M. L. Daroux, P. W. Faguy, E. Yeager, *J. Electrochem. Soc.* **1988**, *135*, 1863–1871.

[8] a) V. S. Bryantsev, F. Faglioni, *J. Phys. Chem. A* **2012**, *116*, 7128–7138; b) V. S. Bryantsev, V. Giordani, W. Walker, M. Blanco, S. Zecevic, K. Sasaki, J. Uddin, D. Addison, G. V. Chase, *J. Phys. Chem. A* **2011**, *115*, 12399–12409; c) M. Carboni, A. G. Marrani, R. Spezia, S. Brutti, *Chem. Eur. J.* **2016**, *22*, 17188–17203; d) A. Khetan, H. Pitsch, V. Viswanathan, *J. Phys. Chem. Lett.* **2014**, *5*, 2419–2424; e) N. Mahne, O. Fontaine, M. O. Thotiyl, M. Wilkening, S. A. Freunberger, *Chem. Sci.* **2017**, *8*, 6716–6729.

[9] a) P. R. Ogilby, *Chem. Soc. Rev.* **2010**, *39*, 3181 – 3209; b) J. Wandt, P. Jakes, J. Granwehr, H. A. Gasteiger, R.-A. Eichel, *Angew. Chem. Int. Ed.* **2016**, *55*, 6892 – 6895; *Angew. Chem.* **2016**, *128*, 7006 – 7009.
[10] N. Mahne, B. Schafzahl, C. Leypold, M. Leypold, S. Grumm, A. Leitgeb, G. A. Strohmeier, M. Wilkening, O. Fontaine, D. Kramer, C. Slugovc, S. M. Borisov, S. A. Freunberger, *Nat. Energy* **2017**, *2*, 17036.
[11] Y. Zhang, L. Ma, L. Zhang, Z. Peng, *J. Electrochem. Soc.* **2016**, *163*, A1270 – A1274.
[12] a) D. H. Chin, G. Chiericato, E. J. Nanni, D. T. Sawyer, *J. Am. Chem. Soc.* **1982**, *104*, 1296 – 1299; b) C. P. Andrieux, P. Hapiot, J. M. Saveant, *J. Am. Chem. Soc.* **1987**, *109*, 3768 – 3775; c) Y. Che, M. Tsushima, F. Matsumoto, T. Okajima, K. Tokuda, T. Ohsaka, *J. Phys. Chem.* **1996**, *100*, 20134 – 20137.
[13] X. Gao, Z. P. Jovanov, Y. Chen, L. R. Johnson, P. G. Bruce, *Angew. Chem. Int. Ed.* **2017**, *56*, 6539 – 6543; *Angew. Chem.* **2017**, *129*, 6639 – 6643.
[14] a) E. J. Corey, M. M. Mehrotra, A. U. Khan, *Biochem. Biophys. Res. Commun.* **1987**, *145*, 842 – 846; b) A. U. Khan, *J. Am. Chem. Soc.* **1981**, *103*, 6516 – 6517; c) W. H. Koppenol, *Nature* **1976**, *262*, 420 – 421; d) E. A. Mayeda, A. J. Bard, *J. Am. Chem. Soc.* **1974**, *96*, 4023 – 4024.

Manuscript received: September 10, 2017
Accepted manuscript online: October 11, 2017
Version of record online: November 2, 2017

